THE JOURNAL OF PHYSICAL CHEMISTRY C

Article

pubs.acs.org/JPCC

Intrinsic Superhydrophilicity of Titania-Terminated Surfaces

Seiji Kawasaki,*[,†,#] Eero Holmström,[‡] Ryota Takahashi,[†,§] Peter Spijker,[‡] Adam S. Foster,[‡,∥] Hiroshi Onishi,[⊥] and Mikk Lippmaa*[,†]

[†]Institute for Solid State Physics, University of Tokyo, 5-1-5 Kashiwanoha, Kashiwa, Chiba 277-8581, Japan

[‡]COMP, Department of Applied Physics, Aalto University, Otakaari 1, FI-00076 Helsinki, Finland

[§]JST PRESTO, 4-1-8 Honcho, Kawaguchi, Saitama 332-0012, Japan

[∥]Division of Electrical Engineering and Computer Science, Kanazawa University, Kanazawa 920-1192, Japan

[⊥]Department of Chemistry, Kobe University, 1-1 Rokkodai, Nada, Kobe 657-8501, Japan

Supporting Information

ABSTRACT: The wettability of solid surfaces is of fundamental scientific interest and related to many diverse chemical and physical phenomena at the heart of practical technologies. In particular, the hydrophilicity of the photocatalytically active metal-oxide TiO_2 has attracted considerable attention for many applications. However, the intrinsic hydrophilicity of Ti-oxide surfaces is not fully understood. In this work, we investigate the intrinsic hydrophilicity of Ti-oxide surfaces on the atomically stable $(\sqrt{13} \times \sqrt{13})$-R33.7° $SrTiO_3$ (001) surface. The surface has a TiO_x double layer on a TiO_2-terminated $SrTiO_3$ (001) surface, which is available as a surface marker to assess the atomic-scale structural stability of the surface. Both experimental and theoretical results show that Ti-oxide surfaces are intrinsically superhydrophilic with a water contact angle of ~0°. The results show that airborne surface contamination is the most significant factor affecting the wettability of titania surfaces, strongly supporting the contamination model for explaining the mechanism of photoinduced superhydrophilicity observed on titanate surfaces. We emphasize that the effect of airborne contamination has to be carefully evaluated when investigating the wettability of surfaces.

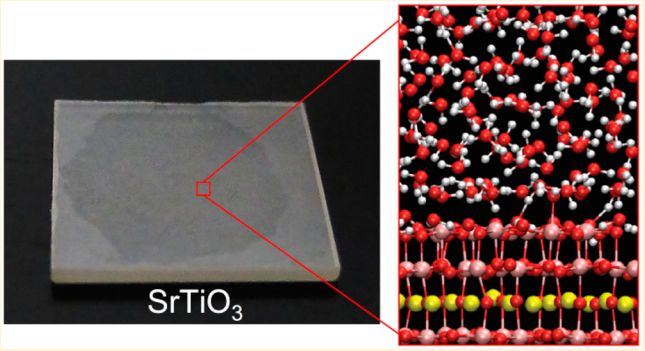

INTRODUCTION

Wettability of solid surfaces is of fundamental chemical and physical interest in adhesion, coatings, and antifouling. It is also an important parameter in microelectronic fabrication and device performance, in energy conversion systems, and in phase change heat transfer.[1] In particular, the interface between titania and water has attracted considerable attention in energy-related research fields, such as the development of photocatalysts,[2] photoelectrochemical[3] and photovoltaic cells,[4] and self-cleaning surfaces.[5] Since the original discovery of photoinduced hydrophilicity,[6] a large number of papers have discussed the mechanism behind the phenomenon,[7] and reported ways of controlling surface wettability by light, heat, and electric field.[8] Due to the inexpensive, abundant, and nontoxic nature of TiO_2, the range of applications of titania has expanded in the past two decades. Nevertheless, the intrinsic hydrophilicity of the TiO_2 surface has proven to be difficult to determine, even though it is a prerequisite for understanding the phenomenon of photoinduced hydrophilicity.

In this work, $(\sqrt{13} \times \sqrt{13})$-R33.7° (hereafter denoted $(\sqrt{13} \times \sqrt{13})$ for brevity) reconstructed $SrTiO_3$ (001) crystals were used as a platform for investigating the intrinsic hydrophilicity of surfaces terminated with a Ti oxide layer. This particular surface reconstruction was found to be atomically stable in water, with water molecules adsorbing molecularly, without chemical reactions. The presence of the $(\sqrt{13} \times \sqrt{13})$ reconstruction can be easily verified by surface diffraction or scanning probe microscopy, making it a convenient marker of an unchanged surface structure when a crystal is exposed to various ambient conditions. While various types of reconstructions have been reported to form on $SrTiO_3$ (001) surfaces,[9−12] the $(\sqrt{13} \times \sqrt{13})$ reconstruction has been recognized as being thermodynamically one of the most stable. The thermodynamic and chemical stability of this reconstruction stems from a TiO_x double layer termination of the $SrTiO_3$ (001) crystal,[13,14] which means that the hydrophilicity characteristics of this surface are not specific to $SrTiO_3$ but can be viewed as being more widely representative of titania-terminated surfaces.

The surface structure and the hydration structure were studied by electron diffraction and atomic force microscopy (AFM). The hydration structure was also simulated by density

Received: December 2, 2016
Revised: January 7, 2017
Published: January 10, 2017

DOI: 10.1021/acs.jpcc.6b12130
J. Phys. Chem. C 2017, 121, 2268−2275

functional theory molecular dynamics (DFT MD) and classical MD. The simulations support the experimental observation that the ($\sqrt{13} \times \sqrt{13}$) $SrTiO_3$ (001) surface is stable in water and displays an extremely low level of dissociative adsorption of water molecules. Despite the weak interaction between the surface and water molecules, the ($\sqrt{13} \times \sqrt{13}$) surface exhibited superhydrophilicity when the surface was clean and protected from airborne contamination. Since ($\sqrt{13} \times \sqrt{13}$) is one of the most stable titania terminated surfaces, most titania terminated surfaces are expected to be intrinsically superhydrophilic. Our results highlight the significant role of ubiquitous airborne surface contaminants in determining the wettability of solid surfaces and show that the effect of contamination cannot be ignored when measuring or discussing the mechanisms of surface hydrophilicity.

METHODS

Experimental Section. $SrTiO_3$ (001) single crystals (Shinkosha) were chemically etched in buffered HF to obtain Sr-free TiO_2-terminated step-and-terrace surfaces.[15,16] The reconstructed ($\sqrt{13} \times \sqrt{13}$) $SrTiO_3$ (001) surfaces[14] were prepared by annealing the wet-etched 0.2° miscut $SrTiO_3$ substrates in a laser heating system that allowed rapid sample temperature changes in an ultrahigh vacuum chamber (background pressure 10^{-8} Torr).[17] The presence of the ($\sqrt{13} \times \sqrt{13}$) reconstruction was verified by reflection high-energy electron diffraction (RHEED), which was performed in the same vacuum chamber at an acceleration voltage of 25 kV and a glancing angle of ~2°. The surface morphology was analyzed in air by amplitude-modulation atomic force microscopy (AM-AFM) while the hydration structure was observed in water by frequency-modulation atomic force microscopy (FM-AFM). The FM-AFM measurements were conducted at 23 °C under atmospheric pressure. During the measurements, a sample and the AFM cantilever were immersed in a 50 mM KCl aqueous solution prepared from KCl (99.5%, Nakarai) and Millipore water. The electrolyte was added in order to reduce the width of the electric double layer near the solid surface (Debye length), which is important for stabilizing the FM-AFM image acquisition.[18] The resonant frequency of the Si cantilever (Nanosensors, NCH) with a nominal spring constant of 40 N m^{-1} was 130−150 kHz and the quality factor (Q) of resonance in water was 10. The water contact angle was evaluated using 2 μL (±0.03 μL) of Millipore water on the sample surface introduced via a micropipette (M & S Instruments, P2) at 20 °C and RH ~ 50%.

Theoretical Calculations. To gain an understanding of the atomic-scale hydration structure of the ($\sqrt{13} \times \sqrt{13}$) surface, we performed quantum-mechanical DFT MD and classical MD simulations of the solid−liquid interface. The DFT MD simulations were performed using the CP2K code.[19] We used the PBE functional[20] with the D3 dispersion correction[21] for exchange and correlation, and a localized Gaussian-type double-ζ basis with polarization orbitals (DZVP) for expanding the electronic orbitals.[22] The simulated $SrTiO_3$ crystal slab had a total thickness of 21 Å in the periodic supercell, with a 14 Å thick layer of water between periodic slab surfaces, adjusted to give overall the experimental density of water (1 g/cm^3). Each slab face comprised one unit cell of the ($\sqrt{13} \times \sqrt{13}$) reconstruction. The time step used in the simulation was 0.5 fs, and the duration of the run was 10 ps, of which the first 5 ps were discarded as an equilibration period. The DFT MD simulation was performed in the NVT ensemble at 300 K using the Nosé−Hoover chain thermostat[23] with three nodes and a time constant of 20 fs to control the temperature.

The classical MD simulations were performed using empirical pair potentials within the LAMMPS code.[24] Interactions between atoms within the crystal were modeled using a Buckingham potential, and crystal-to-water interactions were computed using a 12−6 Lennard-Jones potential.[25] The TIP3P[26] model was used for bulk water. The periodic simulation comprised a ($\sqrt{13} \times \sqrt{13}$)-terminated $SrTiO_3$ (001) slab of 3 nm thickness with 2 × 2 unit cells of the reconstruction on each surface, and a 14 nm layer of bulk water between the slab surfaces. The simulation was run for 0.5 ns with a time step of 1 fs in the NPT ensemble at 300 K at ambient pressure using the Nosé−Hoover chain thermostat. Details of the classical simulation setup can be found in the Supporting Information.

RESULTS AND DISCUSSION

Surface Characterization. The ($\sqrt{13} \times \sqrt{13}$) $SrTiO_3$ (001) surface was reproducibly obtained by a multistep annealing procedure illustrated in Figure 1a. Following the recipe reported in ref 14, a $SrTiO_3$ (001) single crystal was first annealed at 500 °C at an oxygen pressure of 10^{-5} Torr for 10 min to remove carbon contamination from the surface. The crystal was then annealed at 850 °C for 30 min to obtain the TiO_x double layer crystal termination and the associated ($\sqrt{13} \times \sqrt{13}$) reconstruction structure, and subsequently heated to 1000 °C for 3 min. The brief high-temperature annealing was

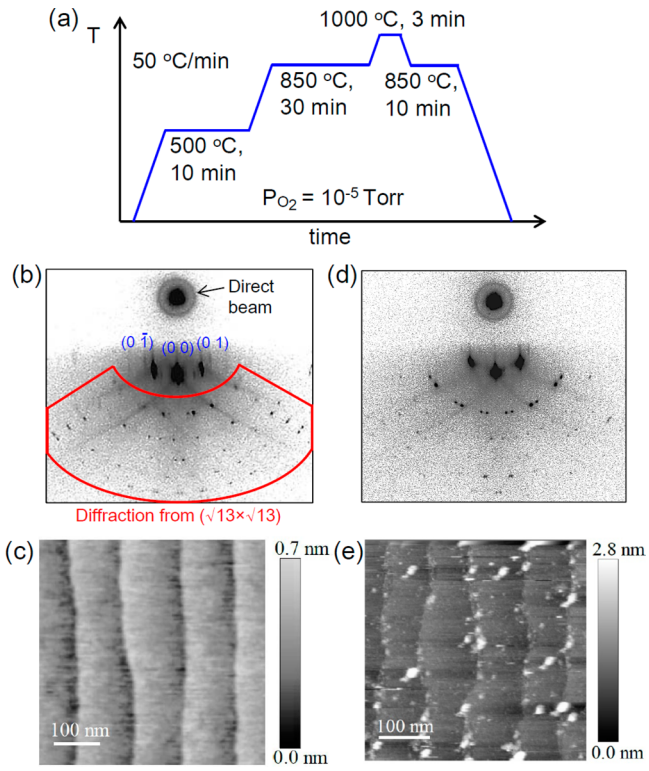

Figure 1. (a) Preparation conditions of a ($\sqrt{13} \times \sqrt{13}$) $SrTiO_3$ (001) surface. RHEED patterns and AFM topographies of ($\sqrt{13} \times \sqrt{13}$) $SrTiO_3$ (001) prepared in a UHV chamber ((b) and (c)) and after water exposure ((d) and (e)). The image in (c) was measured in air using AM-AFM. The image in (e) was measured in a 50 mM KCl aqueous solution with FM-AFM (Δf = 130 Hz).

DOI: 10.1021/acs.jpcc.6b12130
J. Phys. Chem. C 2017, 121, 2268−2275

important for sharpening the step edges, while still keeping the oxygen vacancy density as low as possible.[14] After the brief high-temperature step, a final anneal at 850 °C was used to stabilize the $(\sqrt{13} \times \sqrt{13})$ structure. The sample heating and cooling rates were 50 °C/min. A characteristic RHEED pattern of the $(\sqrt{13} \times \sqrt{13})$ reconstruction observed after cooling to room temperature is shown in Figure 1b. The pattern is consistent with earlier reports.[14,27] The region where the higher-order diffraction spots associated with the $(\sqrt{13} \times \sqrt{13})$ periodicity appear is marked with a red line in Figure 1b. The (0 0), (0 1), and (0 $\bar{1}$) diffraction spots on the zero-order Laue circle belong to the underlying (1 × 1) lattice of the $SrTiO_3$ crystal. A typical RHEED pattern of nonreconstructed $SrTiO_3$ (001) is shown in Figure S4. The step-and-terrace morphology was clearly observed by AM-AFM (Figure 1c). The step height was 4 Å, corresponding to the lattice constant of $SrTiO_3$ (a = 3.905 Å).

The stability of the atomic structure of the $(\sqrt{13} \times \sqrt{13})$ reconstruction upon exposure to water and air was confirmed by RHEED and AFM. Figure 1d shows the RHEED pattern observed after immersing a $(\sqrt{13} \times \sqrt{13})$ reconstructed $SrTiO_3$ crystal in water at 20 °C for 1 h and reloading the sample back into the vacuum chamber. Although the RHEED intensity became weaker after water and air exposure, the characteristic RHEED pattern of the $(\sqrt{13} \times \sqrt{13})$ surface remained visible even after the water exposure (Figure 1d), indicating that the atomic order of the $(\sqrt{13} \times \sqrt{13})$ reconstruction is stable and no structural degradation occurs even on a single atomic layer scale at the surface. The excellent stability of the $(\sqrt{13} \times \sqrt{13})$ reconstruction is quite unusual. Although several types of reconstructions are known to form upon annealing $SrTiO_3$ (001) surfaces, many of the reconstructions are related to the segregation of Sr on the surface.[9−12] Since Sr is rapidly removed from the surface by water exposure,[28] such reconstructions are fragile (See Figure S5). The reason for the intensity change in the RHEED pattern is surface contamination. As can be seen from the FM-AFM image in Figure 1e, the step-and-terrace structure was stable in water despite slight particulate contamination.

The robustness of the $(\sqrt{13} \times \sqrt{13})$ structure may be attributed to the unique TiO_x network on the surface. The $(\sqrt{13} \times \sqrt{13})$ structure is composed of a TiO_x double layer that terminates the crystal with a two-dimensional tiling of edge- or corner-sharing TiO_5 units,[13] as illustrated by VESTA[29] in Figure 2a, stabilizing the dangling bonds on the surface. As suggested by RHEED, the fact that the $(\sqrt{13} \times \sqrt{13})$ atomic structure remains intact even in water was confirmed by FM-AFM. Figure 2b shows a topographic FM-AFM image of the $(\sqrt{13} \times \sqrt{13})$ surface measured in water. The atomic-scale structure was not clear in the raw topographic image, but 4-fold symmetric spots with 1.4 nm periodicity, consistent with the $(\sqrt{13} \times \sqrt{13})$ structure, were clearly observed in a two-dimensional Fourier-transformed image (Figure 2c). A low-pass filtered image (Figure 2d) that was restored by an inverse Fourier transform of the data shown in Figure 2e, showed the expected 1.4 nm periodicity and the 33.7° lattice rotation from the $SrTiO_3$ [100] direction corresponding to the expected $(\sqrt{13} \times \sqrt{13})$-R33.7° structure. We therefore conclude that the atomic structure of the $(\sqrt{13} \times \sqrt{13})$ reconstructed $SrTiO_3$ (001) surface is stable in water, as confirmed by ex situ RHEED and in situ AFM observations.

Hydration Structure. The relationship between macroscopic hydrophilicity and the microscopic hydration structure is

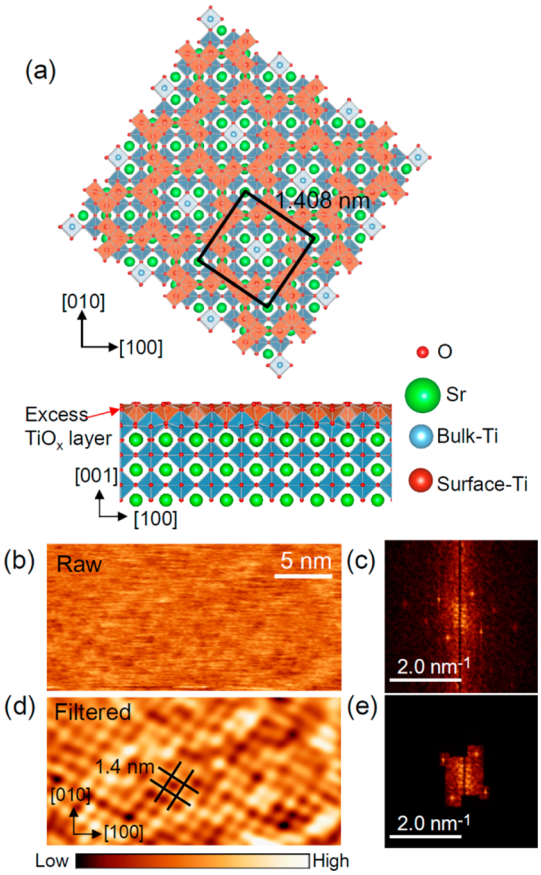

Figure 2. (a) Schematic structure of the $(\sqrt{13} \times \sqrt{13})$ $SrTiO_3$ (001) surface. (b) FM-AFM topography of a $(\sqrt{13} \times \sqrt{13})$ $SrTiO_3$ (001) surface measured in a 50 mM KCl aqueous solution. The cantilever oscillation amplitude and frequency shift were 0.2 nm and +150 Hz, respectively. (c) Fourier-transformed image of (b). (e) Filtered Fourier image with high-frequency components removed and (d) a real-space image obtained by an inverse Fourier transform of (e).

of great scientific interest. Here, the hydration structure of $(\sqrt{13} \times \sqrt{13})$ $SrTiO_3$ (001) was investigated by FM-AFM. The FM-AFM technique has been developed in recent years to a level where three-dimensional solvation structures can be visualized on the atomic scale.[30] The resonance frequency shift (Δf) of the cantilever in FM-AFM, which is often observed at liquid/solid interfaces, reflects the local density distribution of the solvent molecules.[18,31] Figure 3a shows a Δf map obtained by measuring the variation of the cantilever frequency shift as a function of distance from the surface and the lateral position on the surface. At least two Δf oscillations can be seen in the vertical direction in the form of lighter and darker horizontal bands in the image (the two minima labeled M1 and M2 are marked with red dotted lines in Figure 3a). The frequency shift oscillations correspond to local density variations that indicate that there are at least two layers of semiordered water molecules, i.e., hydration layers above the solid surface. Figure 3b shows the Δf-distance curve after averaging over the lateral direction and the corresponding force−distance curve derived using the Sader equation.[32] Force oscillations were observed near the $SrTiO_3$ surface, with force minima located at ∼0.2 and ∼0.5 nm from the surface. The oscillation period (the distance between M1 and M2) in the force curve was ∼0.3 nm, which is in good agreement with the expected thickness of a water molecule layer (0.2−0.4 nm).[30,33] It should be noted that the

DOI: 10.1021/acs.jpcc.6b12130
J. Phys. Chem. C 2017, 121, 2268−2275

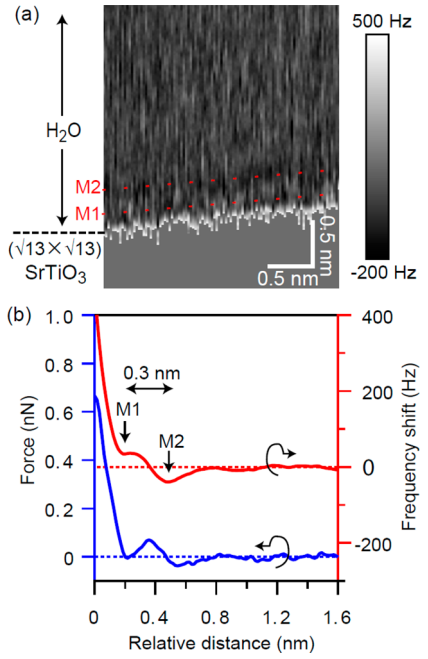

Figure 3. (a) FM-AFM Δf distribution observed above the $(\sqrt{13} \times \sqrt{13})$ $SrTiO_3$ (001) surface in a 50 mM KCl aqueous solution. The slight upward tilt of the water-surface contact line in the lateral direction is caused by microscope drift. (b) A laterally averaged force–distance curve (red) and the corresponding Δf-distance plot (blue). The cantilever oscillation amplitude was 0.1 nm.

surface hydrophilicity determined from the water contact angle varied among several $(\sqrt{13} \times \sqrt{13})$ $SrTiO_3$ samples that were studied. The hydration layer contrast seen in FM-AFM maps correlated directly with the level of contamination of the surface and the hydrophilicity of a particular sample. Only clean surfaces showed a clearly visible hydration structure as in Figure 3a. Surfaces contaminated by long air exposure were always weakly hydrophilic, and the contrast of the hydration structure was weak or unobservable.

The FM AFM measurements of the hydration structure of $SrTiO_3$ were complemented by DFT MD simulations. Figure 4 shows a snapshot of the simulation supercell consisting of the interface between water and the $SrTiO_3$ (001) surface. The

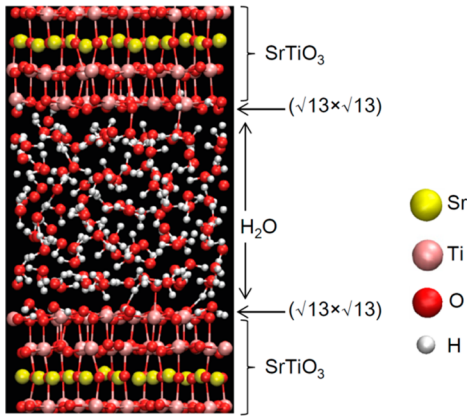

Figure 4. Snapshot of the DFT MD simulation cell comprising the interface between water and the $(\sqrt{13} \times \sqrt{13})$ $SrTiO_3$ (001) surface. Yellow, pink, red, and white spheres represent Sr, Ti, O, and H, respectively.

degree of dissociation was found to be negligibly small on the $(\sqrt{13} \times \sqrt{13})$ surface, and no stable surface hydroxyl groups were formed, indicating that water molecules adsorb molecularly onto the $(\sqrt{13} \times \sqrt{13})$ $SrTiO_3$ surface. In contrast, a high degree of dissociation of water and hence surface hydroxylation was observed on (1×1)-terminated $SrTiO_3$ (001) surfaces for both the TiO_2 and SrO terminations.[34] This finding implies that the chemical stability of the $(\sqrt{13} \times \sqrt{13})$ structure is high, as suggested by the experimental RHEED and AFM finding that the atomic structure of the surface was preserved even after soaking a crystal in water. The fact that water does not dissociate on the $(\sqrt{13} \times \sqrt{13})$ surface structure to any appreciable degree suggests that the interaction between water and the $(\sqrt{13} \times \sqrt{13})$ surface is driven by physical interactions, comprising van der Waals (VDW) forces and hydrogen bonding rather than chemical adsorption. This inference of physisorption is reflected in the adsorption energy of only 0.3 to 0.6 eV for a molecule of H_2O onto the $(\sqrt{13} \times \sqrt{13})$ surface, as computed from static DFT simulations (see the Supporting Information for details). Figure 5a shows the time-averaged atomic density profiles of Sr, Ti, and O of $SrTiO_3$ as well as hydrogen (H_w) and oxygen (O_w) in the liquid region at the interface between water and the $(\sqrt{13} \times \sqrt{13})$ $SrTiO_3$ (001) surface, together with water density profiles, as found by DFT MD. The water density profile shows two water layers with a spacing of 0.26 nm near the surface, in good agreement with the experimental result of 0.3 nm for the distance between the first two minima in the force curve (Figure 3b). A more direct comparison between simulation and experiment can be made by computing an approximate AFM force curve from the equilibrium water density using the solvent-tip approximation (STA).[35,36] The result is shown in Figure 5b, where the analysis is performed on the classical MD trajectory, because this trajectory yields very similar results, yet much improved statistics over the DFT MD one, due to the significantly longer simulation times accessible to classical simulations (see the Supporting Information). The distance between the second and third minima in the force curve in the hydration region is 0.27 nm, in similarly good agreement with experiment as the direct layer-to-layer distance determined from the density alone. In Figure 5c, we visualize the lateral distribution of oxygen ions in the first hydration layer (z = 5 to 8 Å) by plotting the histogram of lateral positions of oxygens in this region. The water molecules largely reside on top of 5-fold coordinated Ti-cations as well as the central cavity of the surface reconstruction. While we find a small accumulation of electronic charge between the Ti cations and the water molecules adsorbed on top of them, the total adsorption energy of only 0.6 eV for this configuration signals physisorption over chemisorption.

Hydrophilicity Measurements. Measuring the degree of intrinsic hydrophilicity of a solid surface can be done by determining the water contact angle. Perfectly clean surfaces can usually be prepared in a vacuum chamber without air or water exposure. However, most reconstructed surfaces that form in vacuum deteriorate rapidly when exposed to water or humidity, which complicates contact angle measurements. Moreover, since the water contact angle is usually measured in air, the measurement results are not reproducible among different experiments as the surfaces are always contaminated by ubiquitous carbonous species in air. This complication has led to a long-standing controversy over the intrinsic hydrophilicity of the Au surface. By carefully analyzing the surface

DOI: 10.1021/acs.jpcc.6b12130
J. Phys. Chem. C 2017, 121, 2268–2275

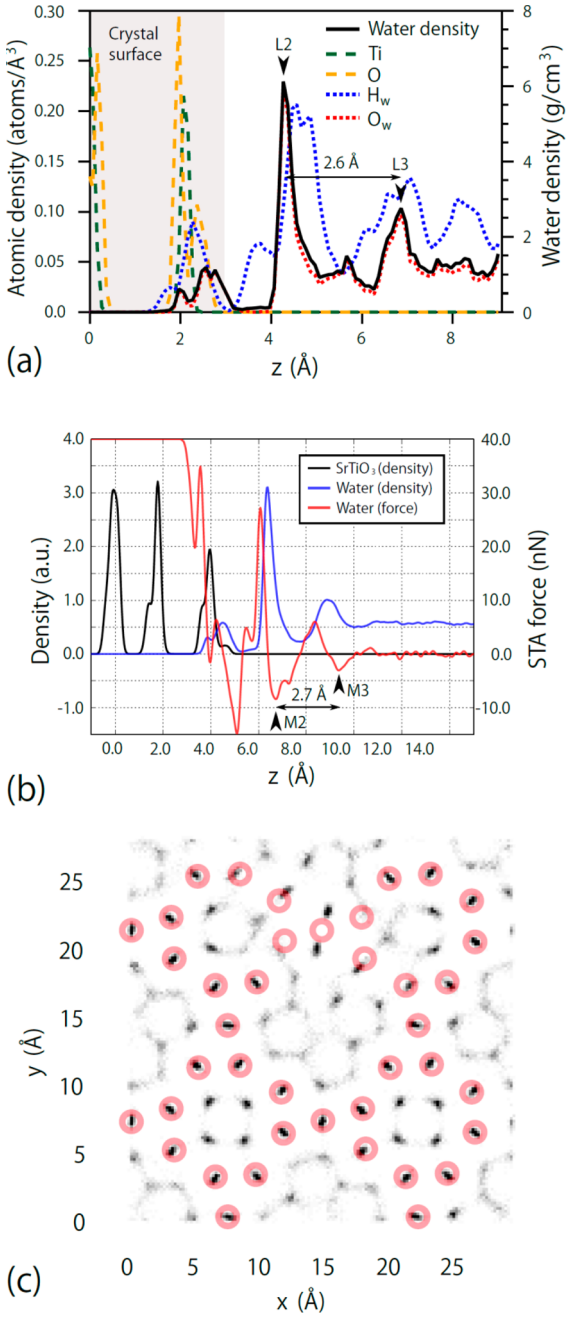

Figure 5. (a) Time-averaged vertical atomic density profiles from the DFT MD simulation. The distance between the first two hydration layers, indicated by L2 and L3, respectively, is 2.7 Å. (b) Average AFM force curve (red line) over the $(\sqrt{13} \times \sqrt{13})$ $SrTiO_3$ (001) surface in water, calculated from the solvent-tip approximation (STA) on the classical MD trajectory. The water and crystal densities are shown for comparison. The second and third force minima in the hydration region are indicated by M2 and M3, respectively, and the distance between them is 2.7 Å. (c) Histogram of lateral positions of oxygens of water molecules in the first hydration layer (z = 5 to 8 Å) from the classical MD trajectory. Underlying 5-fold coordinated Ti cations are shown as pink circles.

contamination and observing a vanishing water contact angle of ~0° within a few minutes of air exposure, Smith finally concluded that the Au surface is intrinsically superhydrophilic.[37] Still, many reports on the hydrophilicity of solid surfaces have ignored the effect of surface contamination when measuring the water contact angle. In fact, the reported values of the water contact angle on TiO_2 (110) in dark conditions varies greatly among experiments from 20° to over 90°.[38−41]

Based on the experimental and theoretical results presented above, $(\sqrt{13} \times \sqrt{13})$ $SrTiO_3$ (001) can be considered to be highly stable against structural deterioration during air and water exposure. The atomic-scale robustness of the surface makes it appropriate for investigating the intrinsic hydrophilicity of titania-terminated surfaces. The water contact angle of the $(\sqrt{13} \times \sqrt{13})$ $SrTiO_3$ surface was measured after different surface treatments, and the results are summarized in Table 1.

Table 1. Water Contact Angle (θ) of the $(\sqrt{13} \times \sqrt{13})$ $SrTiO_3$ (001) Surface for Various Surface Treatments Prior to Contact Angle Measurement[a]

sample	treatment after preparing a $(\sqrt{13}\times\sqrt{13})$ $SrTiO_3$ (001) surface	θ (deg)	surface residues[b]
(A)	exposed to air for <1 min	<4	Sr, V_O
(B)	exposed to air for 1 day	30	Sr, V_O, C
(C)	annealed at 600 °C, $P(O_2) = 10^{-1}$ Torr for 1 h, and exposed to air for <1 min	<4	Sr
(D)	after removing water on (C) by N_2-flow, exposed to air for 10 min	20	Sr, C
(E)	etched in hot water (~60 °C) for 10 min, and dipped in water for cooling to r.t.	<4	V_O
(F)	after removing water on (E) by N_2-flow, exposed to air for 10 min	20	V_O, C
(G)	annealed (F) at 600 °C, $P(O_2) = 10^{-1}$ Torr for 1 h, and exposed to air for <1 min	<4	(clean)
(H)	after removing water on (G) by N_2-flow, exposed to air for 10 min	20	C

[a]Conditions: temperature 20 °C, RH ~ 50%, water 2 μL. [b]Sr and V_O represent Sr-atoms and oxygen vacancies existing on the surface, respectively. C represents carbonous compounds derived from air exposure.

The water contact angle of sample (A) was measured within 1 min of air exposure after preparation of the $(\sqrt{13} \times \sqrt{13})$ surface in a vacuum chamber through the process illustrated in Figure 1a. In order to eliminate the effect of the sample temperature on the contact angle, the sample was cooled to room temperature before the measurement by storing the sample in the vacuum chamber for over 12 h. Sample (A) showed a water contact angle of <4°. The range below 4° is the lower limit of measurable water contact angle,[40] and hence, surfaces with water contact angles below 4° were classified as superhydrophilic in this study. Sample (B) was otherwise identical to (A), except that (B) was kept in air for over 1 day prior to measurement of the contact angle. The contact angle for (B) was ~30°, which indicates that the air exposure destroyed the superhydrophilic state. Air exposure contaminates a solid surface with carbonous species, so sample (B) can be assumed to have been coated with carbon-related contamination.

To prove that the observed superhydrophilicity of sample (A), which was prepared by annealing at 1000 °C and 10^{-5} Torr of oxygen, is an intrinsic property of the $(\sqrt{13} \times \sqrt{13})$ $SrTiO_3$ surface, we had to consider the effects of oxygen vacancies and possible segregated Sr on the surface.[16] To check the effect of oxygen vacancies on the hydrophilicity of a $SrTiO_3$ surface, an as-prepared $(\sqrt{13} \times \sqrt{13})$ $SrTiO_3$ sample was postannealed at 600 °C and 10^{-1} Torr for 1 h prior to measuring the contact angle (sample (C)). These annealing

DOI: 10.1021/acs.jpcc.6b12130
J. Phys. Chem. C 2017, 121, 2268−2275

conditions are optimal for removing oxygen vacancies without degrading the atomic structure of the $(\sqrt{13} \times \sqrt{13})$ $SrTiO_3$ surface. Sample (C) was also superhydrophilic, with a water contact angle below 4°, but subsequent 10 min of air exposure (sample (D)) again destroyed the superhydrophilic state, increasing the water contact angle to ∼20°. Even 10 min of air exposure was thus sufficient to deteriorate the superhydrophilic state, as was the case for the Au surface,[37] but we can conclude that any oxygen vacancies that might have been present in the surface layer after preparing the reconstructed surface did not affect the hydrophilicity.

Annealing $SrTiO_3$ in oxidizing conditions tends to cause Sr segregation to the crystal surface. Segregated Sr thus coexists on the $(\sqrt{13} \times \sqrt{13})$ $SrTiO_3$ surface and may affect the water contact angle. It has been reported that hot water can remove surface Sr species from the $SrTiO_3$ surface.[42] Any Sr residue that had been on the surface of sample (A) was therefore removed by hot water soaking (>60 °C; see Figure S5), leading to sample (E). The surface of sample (E) was still highly hydrophilic, meaning that the $(\sqrt{13} \times \sqrt{13})$ $SrTiO_3$ surface is superhydrophilic regardless of the existence of segregated Sr clusters on the surface. Similarly to sample (D), the superhydrophilicity of sample (E) was destroyed by air exposure (sample (F)). By annealing sample (F) at 600 °C and 10^{-1} Torr for 1 h (G), the surface carbonous contamination and oxygen vacancies were removed to the extent possible without triggering Sr segregation.[15] Sample (G) was the cleanest $(\sqrt{13} \times \sqrt{13})$ $SrTiO_3$ surface considered here, having minimal Sr-related residues, carbonous contamination, or oxygen vacancies. As expected, sample (G) was superhydrophilic, but after 10 min of air exposure, the hydrophilicity decreased (H), as shown in Figure 6. The

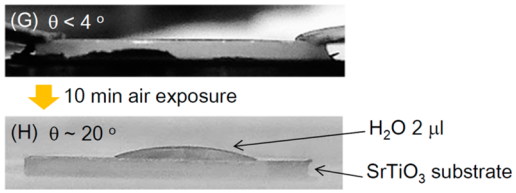

Figure 6. Images of a water droplet on $SrTiO_3$ surface corresponding to the conditions of (G) and (H) described in Table 1.

conclusion from these experiments is that all samples exposed to air for more than about 10 min were weakly hydrophilic, whereas clean samples showed superhydrophilicity just after unloading from the vacuum chamber. The results clearly show that air exposure is the dominant effect for degrading the superhydrophilicity of $(\sqrt{13} \times \sqrt{13})$ $SrTiO_3$ surfaces, and that the degradation is not related to a structural change, e.g., formation of surface OH groups, in the terminating layer of the crystal.

To further support the above analysis, we link our MD simulations to the predicted contact angle of the surface. In general, the contact angle θ is given by Young's equation as

$$\gamma_S = \gamma_L + \gamma_{SL}\cos\theta \quad (1)$$

where γ_S and γ_L are the solid−vapor and the liquid−vapor interfacial (free) energies, respectively, and γ_{SL} is the interfacial energy of the solid−liquid interface. The spreading parameter S is defined as

$$S = \gamma_S - (\gamma_L + \gamma_{SL}) \quad (2)$$

From simple thermodynamic considerations, $S < 0$ means partial wetting of the surface, while $S > 0$ corresponds to the condition of superwetting with $\theta = 0$. Based on our DFT MD simulations of the $(\sqrt{13} \times \sqrt{13})$ $SrTiO_3$ surface with and without water, as well as a simulated system of pure liquid water, the solid−vapor interfacial energy (surface energy) of the isolated $(\sqrt{13} \times \sqrt{13})$ $SrTiO_3$ surface without the entropic contribution is 822 mJ/m^2 at 300 K, and the interfacial energy of the crystal with water is 404 mJ/m^2. From experiment, the liquid−vapor free energy of water (or surface tension) is 72 mJ/m^2 at T = 300 K,[43] which gives a spreading parameter of ∼340 mJ/m^2 ($S \gg 0$) for water on $(\sqrt{13} \times \sqrt{13})$ $SrTiO_3$ (001). To quantify the effect of entropy on this analysis, we assume that upon adsorption onto the oxide surface, the entropy of water cannot decrease more than it does upon freezing of the liquid (-2.3×10^{-4} eV/K/molecule). With this assumption, we find a lower limit of 1 mJ/m^2 for S. Hence, our DFT MD simulations predict superhydrophilicity of the surface, in agreement with the present experimental results (see the Supporting Information for a discussion on the accuracy of this result).

The $(\sqrt{13} \times \sqrt{13})$ $SrTiO_3$ (001) surface is thermodynamically one of the most stable titanate surfaces.[13] As most ionic crystals have a high surface energy, the fact that $(\sqrt{13} \times \sqrt{13})$ $SrTiO_3$ (001) shows superhydrophilicity indicates that Ti oxides and other ionic crystals in general are superhydrophilic, independent of the surface structure. To test this prediction, we measured the water contact angle on $SrTiO_3$ with other surface terminations and several other oxide surfaces (TiO_2, Al_2O_3, and $NdGaO_3$) and found that these surfaces are also superhydrophilic if the surfaces are free from contamination caused by air exposure (see Figures S6 and S7).

Photoinduction. Finally, we discuss the mechanism of photoinduced superhydrophilicity observed on titanate surfaces. There is a long-standing controversy on the mechanism behind this effect. Two competing hypotheses have been proposed. The first one is the "surface reconstruction model", which explains the strong hydrophilicity by the appearance of a surface reconstruction induced by a reaction of the crystal surface with water under light exposure.[44] The second hypothesis is a "contamination model", which considers photocatalytic decomposition of organic contaminants on the surface as the main factor governing the phenomenon of photoinduced hydrophilicity, since the hydrophilicity of most clean oxide surfaces should be intrinsically very high due to the large surface energy.[40,45] Several other proposals have also been discussed.[46,47] Based on our results presented above, bare titania-terminated surfaces are intrinsically superhydrophilic, as long as the surfaces are not exposed to airborne contamination. This finding clearly supports the contamination model. Although surface reconstructions such as surface hydroxyl groups and light-induced oxygen vacancy formation may affect the hydrophilicity, the appearance of hydrophilicity under light irradiation can be fully understood by the contamination model without having to assume a structural change at the surface. This conclusion is supported by results of several in situ spectroscopic studies.[40,41,45,48−50]

CONCLUSION

The atomic structure of the $(\sqrt{13} \times \sqrt{13})$ $SrTiO_3$ (001) surface was found to be highly stable against air and water exposure, with water molecules adsorbing onto the surface with a negligible degree of dissociation. By utilizing the $(\sqrt{13} \times$

DOI: 10.1021/acs.jpcc.6b12130
J. Phys. Chem. C 2017, 121, 2268−2275

$\sqrt{13}$) structure as a stable surface marker, the intrinsic hydrophilicity of a titania-terminated surface was investigated. The surfaces were thermodynamically stable intrinsically and superhydrophilic as long as the surface was clean and not exposed to airborne contamination. This is likely independent of a particular surface reconstruction, crystal plane, or dopants. We thus conclude that titanate surfaces are intrinsically superhydrophilic due to their high surface energy. This finding strongly supports the contamination model for explaining the mechanism of photoinduced superhydrophilicity observed on titanate surfaces. Our results highlight the critical role of airborne contamination for surface wettability, although the role of such contamination has often been ignored in discussions of hydrophilicity and contact angle measurements. We emphasize that the effect of surface contamination has to be carefully evaluated when investigating the intrinsic hydrophilicity of oxide crystal surfaces.

■ ASSOCIATED CONTENT

Supporting Information

The Supporting Information is available free of charge on the ACS Publications website at DOI: 10.1021/acs.jpcc.6b12130.

Details of the simulations, static DFT results on adsorption of water onto ($\sqrt{13} \times \sqrt{13}$), the water contact angle on various oxide surfaces, and discussion on the contact angle calculations from simulation results (PDF)

■ AUTHOR INFORMATION

Corresponding Authors

*E-mail: skawasaki@sci-res.net.

*E-mail: mlippmaa@issp.u-tokyo.ac.jp. Tel: +81-4-7136-3315.

ORCID

Seiji Kawasaki: 0000-0003-0479-5923

Adam S. Foster: 0000-0001-5371-5905

Present Address

#Materials Sciences Division, Lawrence Berkeley National Laboratory, 1 Cyclotron Road, Berkeley, California 94720, United States.

Author Contributions

S.K. performed all the experiments and classical MD simulations. E.H. simulated the interface of water and $SrTiO_3$ by DFT. R.T, H.O., and M.L. supported the experiments, while P.S. and A.S.F. supported the simulations. The manuscript was written through contributions of all authors.

Notes

The authors declare no competing financial interest.

■ ACKNOWLEDGMENTS

S.K. was supported by the Japan Society for the Promotion of Science (JSPS) and the Program for Leading Graduate Schools (MERIT). Prof. Katsuyuki Fukutani, Prof. Fumio Komori, Prof. Yuji Matsumoto, Prof. Maki Kawai, and Dr. Ryota Shimizu are acknowledged for fruitful discussion. The FM-AFM used in this study was developed by the Advanced Measurement and Analysis Project of the Japan Science and Technology Agency. Dr. Yuki Araki, Mr. Shunsuke Suiko, and Mr. Yusuke Tanaka are acknowledged for optimizing the FM-AFM equipment. E.H., P.S., and A.S.F. acknowledge financial support by the Academy of Finland through the Centres of Excellence Program (Project No. 251748) and generous grants of computing time from CSC − IT Center for Science, Finland. The work was supported in part by JSPS kakenhi Grant No. 26105002.

■ REFERENCES

(1) Attinger, D.; Frankiewicz, C.; Betz, A. R.; Schutzius, T. M.; Ganguly, R.; Das, A.; Kim, C.-J.; Megaridis, C. M. Surface engineering for phase change heat transfer: A review. *MRS Energy & Sustainability* **2014**, *1*, 1−40.

(2) Fujishima, A.; Zhang, X.; Tryk, D. A. TiO_2 Photocatalysis and Related Surface Phenomena. *Surf. Sci. Rep.* **2008**, *63*, 515−582.

(3) Grätzel, M. Photoelectrochemical Cells. *Nature* **2001**, *414*, 338−344.

(4) Hagfeldt, A.; Boschloo, G.; Sun, L.; Kloo, L.; Pettersson, H. Dye-sensitized Solar Cells. *Chem. Rev.* **2010**, *110*, 6595−6663.

(5) Banerjee, S.; Dionysiou, D. D.; Pillai, S. C. Self-cleaning Applications of TiO_2 by Photo-Induced Hydrophilicity and Photocatalysis. *Appl. Catal., B* **2015**, *176−177*, 396−428.

(6) Wang, R.; Hashimoto, K.; Fujishima, A.; Chikuni, M.; Kojima, E.; Kitamura, A.; Shimohigoshi, M.; Watanabe, T. Light-induced Amphiphilic Surfaces. *Nature* **1997**, *388*, 431−432.

(7) Zhang, L.; Dillert, R.; Vormoor, M. Photo-induced Hydrophilicity and Self-cleaning: Models and Reality. *Energy Environ. Sci.* **2012**, *5*, 7491−7507.

(8) Verplanck, N.; Coffinier, Y.; Thomy, V.; Boukherroub, R. Wettability Switching Techniques on Superhydrophobic Surfaces. *Nanoscale Res. Lett.* **2007**, *2*, 577−596.

(9) Kubo, T.; Nozoye, H. Surface structure of $SrTiO_3$(1 0 0) Original Research Article. *Surf. Sci.* **2003**, *542*, 177−191.

(10) Kienzle, D. M.; Marks, L. D. Surface Transmission Electron Diffraction for $SrTiO_3$ Surfaces. *CrystEngComm* **2012**, *14*, 7833−7839.

(11) Shiraki, S.; Nantoh, M.; Katano, S.; Kawai, M. Nanoscale Structural Variation Observed on the Vicinal $SrTiO_3$ (001) Surface. *Appl. Phys. Lett.* **2010**, *96*, 231901.

(12) Castell, M. R. Scanning Tunneling Microscopy of Reconstructions on the $SrTiO_3$(0 0 1). *Surf. Sci.* **2002**, *505*, 1−13.

(13) Kienzle, D. M.; Becerra-Toledo, A. E.; Marks, L. D. Vacant-Site Octahedral Tilings on $SrTiO_3$ (001), the ($\sqrt{13}\times\sqrt{13}$) *R*33.7° Surface, and Related Structures. *Phys. Rev. Lett.* **2011**, *106*, 176102.

(14) Shimizu, R.; Iwaya, K.; Ohsawa, T.; Shiraki, S.; Hasegawa, T.; Hashizume, T.; Hitosugi, T. Atomic-Scale Visualization of Initial Growth of Homoepitaxial $SrTiO_3$ Thin Film on an Atomically Ordered Substrate. *ACS Nano* **2011**, *5*, 7967−7971.

(15) Kawasaki, M.; Takahashi, K.; Maeda, T.; Shinohara, M.; Ishiyama, O.; Yonezawa, T.; Yoshimoto, M.; Koinuma, H. Atomic Control of the $SrTiO_3$ Crystal Surface. *Science* **1994**, *266*, 1540.

(16) Ohnishi, T.; Shibuya, K.; Lippmaa, M.; Kobayashi, D.; Kumigashira, H.; Oshima, M. Preparation of Thermally Stable TiO_2-terminated $SrTiO_3$ (100) Substrate Surfaces. *Appl. Phys. Lett.* **2004**, *85*, 272.

(17) Ohashi, S.; Lippmaa, M.; Nakagawa, N.; Nagasawa, H.; Koinuma, H.; Kawasaki, M. Compact Laser Molecular Beam Epitaxy System Using Laser Heating of Substrate for Oxide Film Growth. *Rev. Sci. Instrum.* **1999**, *70*, 178.

(18) Hiasa, T.; Kimura, K.; Onishi, H.; Ohta, M.; Watanabe, K.; Kokawa, R.; Oyabu, N.; Kobayashi, K.; Yamada, H. Aqueous Solution Structure over α-Al_2O_3 (01$\bar{1}$2) Probed by Frequency-Modulation Atomic Force Microscopy. *J. Phys. Chem. C* **2010**, *114*, 21423−21426.

(19) CP2K Open Source Molecular Dynamics, http://www.cp2k.org.

(20) Perdew, J. P.; Burke, K.; Ernzerhof, M. Generalized Gradient Approximation Made Simple [Phys. Rev. Lett. 77, 3865 (1996)]. *Phys. Rev. Lett.* **1997**, *78*, 1396.

(21) Grimme, S.; Antony, J.; Ehrlich, S.; Krieg, H. A Consistent and Accurate ab initio Parametrization of Density Functional Dispersion Correction (DFT-D) for the 94 Elements H-Pu. *J. Chem. Phys.* **2010**, *132*, 154104.

DOI: 10.1021/acs.jpcc.6b12130
J. Phys. Chem. C 2017, 121, 2268−2275

(22) VandeVondele, J.; Hutter, J. Gaussian Basis Sets for Accurate Calculations on Molecular Systems in Gas and Condensed Phases. *J. Chem. Phys.* **2007**, *127*, 114105.
(23) Martyna, G. J.; Klein, M. L.; Tuckerman, M. Nosé−Hoover Chains: The Canonical Ensemble via Continuous Dynamics. *J. Chem. Phys.* **1992**, *97*, 2635.
(24) Plimpton, S. Fast Parallel Algorithms for Short-Range Molecular Dynamics. *J. Comput. Phys.* **1995**, *117*, 1−19.
(25) Lukyanov, S. I.; Bandura, A. V.; Evarestov, R. A. Fast Parallel Algorithms for Short-Range Molecular Dynamics. *Surf. Sci.* **2013**, *611*, 10−24.
(26) Jorgensen, W. L.; Chandrasekhar, J.; Madura, J. D.; Impey, R. W.; Klein, M. L. Comparison of Simple Potential Functions for Simulating Liquid Water. *J. Chem. Phys.* **1983**, *79*, 926−935.
(27) Naito, M.; Sato, H. Reflection High-Energy Electron Diffraction Study on the $SrTiO_3$ Surface Structure. *Phys. C* **1994**, *229*, 1−11.
(28) Koster, G.; Kropman, B. L.; Rijinders, G. J. H. M.; Blank, D. H. A.; Rogalla, H. Quasi-ideal Strontium Titanate Crystal Surfaces through Formation of Strontium Hydroxide. *Appl. Phys. Lett.* **1998**, *73*, 2920.
(29) Momma, K.; Izumi, F. VESTA: a Three-dimensional Visualization System for Electronic and Structural Analysis. *J. Appl. Crystallogr.* **2008**, *41*, 653−658.
(30) Fukuma, T. Water Distribution at Solid/liquid Interfaces Visualized by Frequency Modulation Atomic Force Microscopy. *Sci. Technol. Adv. Mater.* **2010**, *11*, 033003.
(31) Kimura, K.; Ido, S.; Oyabu, N.; Kobayashi, K.; Hirata, Y.; Imai, T.; Yamada, H. Visualizing Water Molecule Distribution by Atomic Force Microscopy. *J. Chem. Phys.* **2010**, *132*, 194705.
(32) Sader, J. E.; Javis, S. P. Accurate Formulas for Interaction Force and Energy in Frequency Modulation Force Spectroscopy. *Appl. Phys. Lett.* **2004**, *84*, 1801−1804.
(33) Fukuma, T.; Reischl, B.; Kobayashi, N.; Spijker, P.; Canova, F. F.; Miyazawa, K.; Foster, A. S. Mechanism of Atomic Force Microscopy Imaging of Three-Dimensional Hydration Structures at a Solid-liquid Interface. *Phys. Rev. B: Condens. Matter Mater. Phys.* **2015**, *92*, 155412.
(34) Holmström, E.; Spijker, P.; Foster, A. S. The Interface of $SrTiO_3$ and H_2O from Density Functional Theory Molecular Dynamics. *Proc. R. Soc. London, Ser. A* **2016**, *472*, 20160293.
(35) Watkins, M.; Reischl, B. A Simple Approximation for Forces Exerted on an AFM Tip in Liquid. *J. Chem. Phys.* **2013**, *138*, 154703.
(36) Miyazawa, K.; Kobayashi, N.; Watkins, M.; Shluger, A. L.; Amano, K.; Fukuma, T. A Relationship between Three-dimensional Surface Hydration Structures and Force Distribution Measured by Atomic Force Microscopy. *Nanoscale* **2016**, *8*, 7334.
(37) Smith, T. The Hydrophilic Nature of a Clean Gold Surface. *J. Colloid Interface Sci.* **1980**, *75*, 51.
(38) Watanabe, T.; Nakajima, A.; Wang, R.; Minabe, M.; Koizumi, S.; Fujishima, A.; Hashimoto, K. Photocatalytic Activity and Photo-induced Hydrophilicity of Titanium Dioxide Coated Glass. *Thin Solid Films* **1999**, *351*, 260−263.
(39) Wang, R.; Sakai, N.; Fujishima, A.; Watanabe, T.; Hashimoto, K. Studies of Surface Wettability Conversion on TiO_2 Single-Crystal Surfaces. *J. Phys. Chem. B* **1999**, *103*, 2188−2194.
(40) Zubkov, T.; Stahl, D.; Thompson, T. L.; Panayotov, D.; Diwald, O.; Yates, J. T., Jr. Ultraviolet Light-Induced Hydrophilicity Effect on $TiO_2(110)(1 \times 1)$. Dominant Role of the Photooxidation of Adsorbed Hydrocarbons Causing Wetting by Water Droplet. *J. Phys. Chem. B* **2005**, *109*, 15454−15462.
(41) Takahashi, K.; Yui, H. Analysis of Surface OH Groups on TiO_2 Single Crystal with Polarization Modulation Infrared External Reflection Spectroscopy. *J. Phys. Chem. C* **2009**, *113*, 20322−20327.
(42) Kobayashi, D.; Hashimoto, R.; Chikamatsu, A.; Kumigashira, H.; Oshima, M.; Ohnishi, T.; Lippmaa, M.; Ono, K.; Kawasaki, M.; Koinuma, H. Sr Surface Segregation and Water Cleaning for Atomically Controlled $SrTiO_3$ (0 0 1) Substrates Studied by Photoemission Spectroscopy. *J. Electron Spectrosc. Relat. Phenom.* **2005**, *144−147*, 443−446.
(43) Floriano, M. A.; Angell, C. A. Surface Tension and Molar Surface Free Energy and Entropy of Water to −27.2.degree.C. *J. Phys. Chem.* **1990**, *94*, 4199−4202.
(44) Sakai, N.; Fujishima, A.; Watanabe, T.; Hashimoto, K. Quantitative Evaluation of the Photoinduced Hydrophilic Conversion Properties of TiO_2 Thin Film Surfaces by the Reciprocal of Contact Angle. *J. Phys. Chem. B* **2003**, *107*, 1028−1035.
(45) Takeuchi, M.; Sakamoto, K.; Martra, G.; Coluccia, S.; Anpo, M. Mechanism of Photoinduced Superhydrophilicity on the TiO_2 Photocatalyst Surface. *J. Phys. Chem. B* **2005**, *109*, 15422−15428.
(46) Langlet, M.; Permpoon, S.; Riassetto, D.; Berthomé, G.; Pernot, E.; Joud, J. C. Photocatalytic Activity and Photo-induced Superhydrophilicity of Sol−gel Derived TiO_2 Films. *J. Photochem. Photobiol., A* **2006**, *181*, 203−214.
(47) Yan, X.; Abe, R.; Ohno, T.; Toyofuku, M.; Ohtani, B. Action Spectrum Analyses of Photoinduced Superhydrophilicity of Titania Thin Films on Glass Plates. *Thin Solid Films* **2008**, *516*, 5872−5876.
(48) Jribi, R.; Barthel, E.; Bluhm, H.; Grunze, M.; Koelsch, P.; Verreault, D.; Søndergård, E. Ultraviolet Irradiation Suppresses Adhesion on TiO_2. *J. Phys. Chem. C* **2009**, *113*, 8273−8277.
(49) White, J. M.; Szanyi, J.; Henderson, M. A. The Photon-Driven Hydrophilicity of Titania: A Model Study Using TiO_2 (110) and Adsorbed Trimethyl Acetate. *J. Phys. Chem. B* **2003**, *107*, 9029−9033.
(50) Uosaki, K.; Yano, T.; Nihonyanagi, S. Interfacial Water Structure at As-prepared and UV-Induced Hydrophilic TiO_2 Surfaces Studied by Sum Frequency Generation Spectroscopy and Quartz Crystal Microbalance. *J. Phys. Chem. B* **2004**, *108*, 19086−19088.

DOI: 10.1021/acs.jpcc.6b12130
J. Phys. Chem. C 2017, 121, 2268−2275